Springer

KSME

Journal of Mechanical Science and Technology 25 (1) (2011) 221~231
www.springerlink.com/content/1738-494x
DOI 10.1007/s12206-010-1104-y

Robust control application for a three-axis road simulator †

J.W. Kim[1], D.J. Xuan[2] and Y.-B. Kim[3,*]

[1]*Advanced Mechatronics Tecnology, Gwangju 500-757, Korea*
[2]*College of Mechanical and Electrical Engineering, Wenzhou University, 325035, China*
[3]*Department of Mechanical Engineering, Chonnam National University, Gwangju, 500-757 Korea*

(Manuscript Received July 25, 2008; Revised June 1, 2010; Acccepted October 3, 2010)

Abstract

This paper presents the design of a quantitative feedback control system for a three-axis hydraulic road simulator. The road simulator is a multiple input-output (MIMO) system with parameter uncertainties which should be compensated with a robust control method. The objective of the present paper is to reproduce the random input signal or real road vibration signal by three hydraulic cylinders. The replaced m^2 MISO equivalent control system is suggested, which satisfies the design specification of the original *mxm* MIMO control system by decoupling each of the three axes. Quantitative Feedback Theory (QFT) is used to control the simulator. The QFT illustrates a tracking performance of the closed-loop controller with low order transfer function *G (s)* and pre-filter *F (s)* having the minimum bandwidth for the uncertain plant with parameter uncertainty. The efficacy of the designed controller is verified through dynamic simulation, which is co-simulated with hydraulic models of Matlab and Adams multi-body. The simulation and the experimental results show that the proposed control technique works well for uncertain hydraulic plant systems.

Keywords: QFT; Dynamic road simulator; Uncertain plant; Hydraulic servo cylinder; Robust control; Force control system

1. Introduction

The vehicle dynamic characteristics and fatigue test are largely classified by two test methods: real road test and lab test, which is done inside of the room by reproducing the real road data. The real road test can afford high reliability as well as credibility on a vehicle's dynamic behaviour and fatigue expectation. However, as it has the disadvantages of time, spatial and environmental limitations as well as dependency on the driver's skill and the environment of the test road , it always requires compensation and continuous observation of the test results. Meanwhile, the lab test can supplement the demerits of the real road test by reproducing the real road input data. Even though it has many disadvantages, such as initial investment of the machine, continuous maintenance and operator education, its usage as a multi-axis hydraulic road simulator has been increasing recently. The main advantages of the simulator are that it can provide very flexible test methods through varied control input with different test specimens, and it can reduce test time and cost with an accelerated vibration test method [1]. Furthermore, one of the most important factors of the road simulatoris how accurately it can reproduce the real road data or random input at the dummy wheel. Each three-axis mechanical movement (longitudinal, lateral and vertical) should have as little interference as possible with other axes of motion (i.e. de-coupled motion) and it should have a reliable structure that can endure severe vibration due to a large external load. Also, it should have the robust control cability to reproduce the precise movements of each of the three axes under the given input data because each test specimen is never the same and the test environment keeps changing.

Basically the three-axis hydraulic road simulator is the uncertain plant, and this uncertainty comes from the mechanical coupling, non-linear hydraulic valve displacement, dynamic loading change and the varaiance of the supply oil pressure. Therefore, in this paper, quantitative feedback theory (QFT), which is one of the modern control techniques available to handle the uncertain plant with external disturbance, is utilized. QFT is the control methodology designed on the frequency domain to cover plant uncertainty and external disturbance [2-7]. It has the advantage of having a lower order controller than other control techniques such as LQG/LTR technology, H_2/H_∞ technology, and synthesis [8-10]. Horowitz (1972) first established the QFT [3], which can be robustly applied in controlling plant uncertainty and external disturbances. Later, Shaked (1976) modified QFT to improve Horowitz's method by transforming the multi-variable plant into a diagonal one

† This paper was recommended for publication in revised form by Associate Editor Kyongsu Yi

*Corresponding author. Tel.: +82 62 530 1677, Fax.: +82 62 530 1689
E-mail address: ybkim@chonnam.ac.kr

[11]. However, his method has the iteration problem to find the loop transfer function with minimum bandwidth. Horowitz (1982) revisited the QFT using the fixed point algorithm for a MIMO LTI system. Yaniv (1986) published the QFT which is much simpler and requires fewer iteration steps than the previous ones, but his method shows a numerical problem for large control systems because the inverse of the transfer function is compulsory. In 1988, D'Azzo and Houpis established the QFT design and analysis by solving the above mentioned problems [5]. Borghesani (1993) made a conventional numerical program for the Matlab toolbox [12, 13]. Using his method, Park (1998) showed the stability with marginal parameter values using the Matlab QFT toolbox [14]. The engineering application area using the QFT is very broad. Many applications, such as automotive dynamics, robotics, aerospace and MEMS area, have been made. In particular, Ahn (2007) utilized the QFT in controlling a hydraulic actuator [15] and Ha (2000) used the QFT in controlling robotics area [16].

The most important factor in QFT is to design a controller satisfying the uncertain plant dynamics and compensating for the external disturbance in the frequency domain. The characteristics of the QFT are to design a lower order controller having minimum bandwidth. By considering the amplitude and phase information simultaneously in the Nichols chart, an optimal controller is designed utilizing loop shaping. After choosing the nominal plant and fulfilling all the boundary conditions, the final controller with lower order transfer function is synthesized. Empirical experience and thorough control knowledge are required for deciding the optimal controller.

The mechanical plant in this paper has three-axis hydraulic road actuators with a dummy wheel. The actuators have three independent orthogonal motions—vertical, longitudinal and lateral movement. The longitudinal and lateral movements use force as a control input and the vertical motion utilizes displacement for actuation. Therefore, the force and displacement actuations should be considered simultaneously. In theory, a x3 controller is required to control the hydraulic simulator, which is considered as a MIMO simulator. However, as the mechanical coupling between each axis is negligible, independent control of the three axes using 3 MISO is possible [7].

The paper consists of the following parts: the characteristics of the three-axis simulator are considered and de-coupling among the three axes is verified in Section 2 while its mathematical justification is covered in Section 3, mathematical modeling of the hydraulic simulator is performed in Section 4, equivalent MISO QFT control synthesis is derived in Section 5, various simulation and experiments are performed and their results are shown in Section 6, and a conclusion is made in Section 7.

2. De-coupling analysis by co-simulation

In order to study the de-coupling effect of each axis, Adams kinematic/dynamic software is simulated, as shown in Fig. 1.

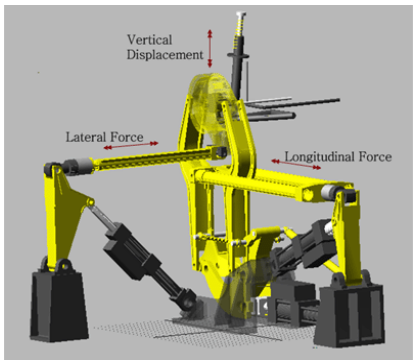

Fig. 1. Adams model of the hydraulic road simulator.

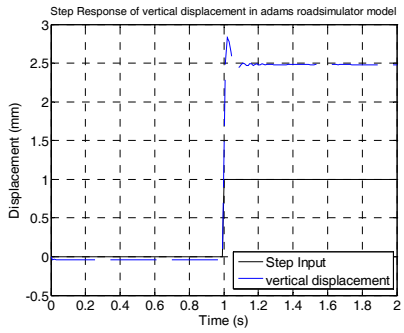

(a) Displacement of vertical axis with step input

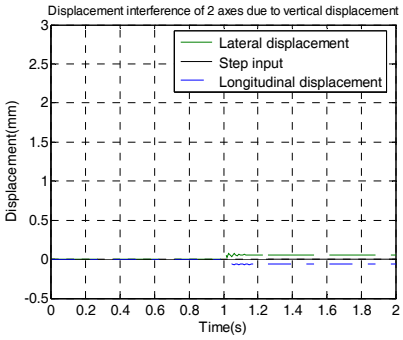

(b) Displacements interference of longitudinal and lateral axis

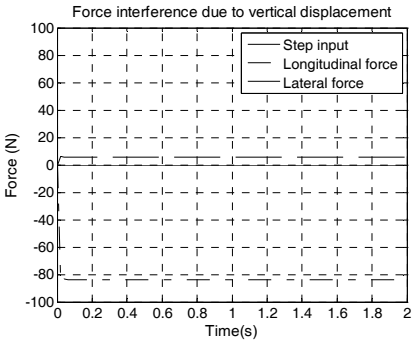

(c) Force interference of longitudinal and lateral axis

Fig. 2. Simulation relating to cross coupling analysis.

The Adams model has a total of 30 DOFs, and it also includes 3 cylindrical joints, 13 revolute joints, 5 spherical joints and 3 Hook's joints. To observe the de-coupling effect of each axis, lateral and longitudinal excitations are made with ±0.05*mm* displacement variations, and vertical excitations are

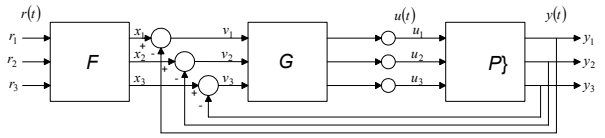

Fig. 3. MIMO feedback control structure.

actuated with ±1*mm* amplitude. The simulation is performed by engaging step input for the vertical axis and having no inputs for the remaining axes. The simulation results are shown in Fig. 2.

Fig. 2(a) shows the result of the displacement of the vertical axis with step input of 1 mm at the cylinder. As its linkage ratio is exactly 2.5, the dummywheel output displacement shows 2.5 *mm* movement exactly. Fig. 2(b) shows the results of the lateral and longitudinal movements due to step input of the vertical one. From the figure, it can be concluded that the coupling ratio between the lateral and longitudinal axes with vertical motion is within 3%, which shows that the coupling effect between the vertical axis and other two axes are almost negligible. Fig. 2(c) shows the force outputs of the two axes (longitudinal and lateral). The force outputs are below 100 *N*, which also shows negligible force interference with vertical one, which requires almost 2000 *N* actuation.

3. Mathematical justification of MISO system

The hydraulic road simulator has three inputs and three outputs, as shown in Fig. 3. In the figure, {*P*} represents the plant dynamics, *G* is a controller and *F* is a pre-filter. The plant dynamics has inherent uncertain parameters such as dynamic load variation and uncertain hydraulic parameters.

In the model, each *F, G* and *P* are described as

$$F=\begin{bmatrix} f_{11} & 0 & 0 \\ 0 & f_{22} & 0 \\ 0 & 0 & f_{33} \end{bmatrix} \quad G=\begin{bmatrix} g_{11} & 0 & 0 \\ 0 & g_{22} & 0 \\ 0 & 0 & g_{33} \end{bmatrix}$$

$$P=\begin{bmatrix} p_{11} & p_{12} & p_{13} \\ p_{21} & p_{22} & p_{23} \\ p_{31} & p_{32} & p_{33} \end{bmatrix}. \tag{1}$$

If there is very small coupling between each simulator axis, the controller *G* and pre-filter *F* can be diagonalized, as represented by Eq. 1 (see Jeong et al. [17]). From the previous research, the control ratio matrix *T* with elements of t_{ij} is the matrix representing the input r_j and output y_i, where *i,j*=1,2,3. Thus,

$$T=\begin{bmatrix} t_{11} & t_{12} & t_{13} \\ t_{21} & t_{22} & t_{23} \\ t_{31} & t_{32} & t_{33} \end{bmatrix} \quad G=\begin{bmatrix} g_{11} & 0 & 0 \\ 0 & g_{22} & 0 \\ 0 & 0 & g_{33} \end{bmatrix}$$

$$Q=P^{-1}=\begin{bmatrix} q_{11} & q_{12} & q_{13} \\ q_{21} & q_{22} & q_{23} \\ q_{31} & q_{32} & q_{33} \end{bmatrix}. \tag{2}$$

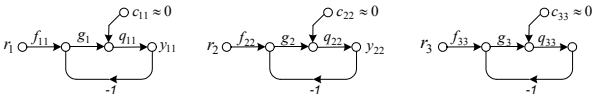

Fig. 4 MISO loops with cross coupling rejection.

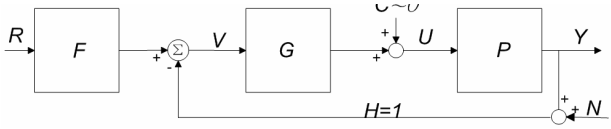

Fig. 5. MISO loops minimizing cross coupling effect.

The MIMO relations from Fig. 3 can be expressed as

$$y=[I+PG]^{-1}PGFr\ . \tag{3}$$

Therefore, the control ratio matrix *T* can be obtained as

$$T=\frac{y}{r}=[I+PG]^{-1}PGF\ . \tag{4}$$

The present paper utilizes a multiple MISO system which is the equivalent of a MIMO system using the relevant mapping with minimum cross-coupling effects. From the previous research results, it is clear that the three-axis simulator's cross-coupling effect between vertical, lateral and longitudinal dynamics is negligible; multiple MISO control instead of a full MIMO one exhibits equivalent control effects with the benefit of simple mathematical derivation.

In Eq. (4), the problem is to design system transfer function t_{ij}, which is very complicated and difficult. However, using Schauder's fixed point algorithm, MIMO can be designed into MISO (Horowitz, [4]). The problem is to find the appropriate mapping, which minimizes the effect of the cross coupling terms, and allows the newly-designed MISO controller to track the desired input.

By using the fixed point algorithm proposed by Schauder and Horowitz, the inverse matrix of P can be easily obtained as

$$P^{-1}=[p_{ij}^{*}]=\left[\frac{1}{q_{ij}}\right]=\Lambda+B$$

where Λ is the matrix with diagonal terms and *B* is the balanced matrix for the offt-diagonal terms, i.e. $i \neq j$.

$$Y(T_i) \equiv [\Lambda+G]^{-1}[GF-BT_i] \equiv T_j \tag{5}$$

For a more detailed derivation of the above equation, please refer to Ref. [5]. Fig. 4 shows the diagonalized input and output relations by neglecting the cross coupling effect. The approximated control dynamics in Fig. 4 can be represented as

$$y_{11}=\frac{f_{11}g_1q_{11}}{1+g_1q_{11}},\ y_{22}=\frac{f_{22}g_2q_{22}}{1+g_2q_{22}},\ y_{33}=\frac{f_{33}g_3q_{33}}{1+g_3q_{33}}. \tag{6}$$

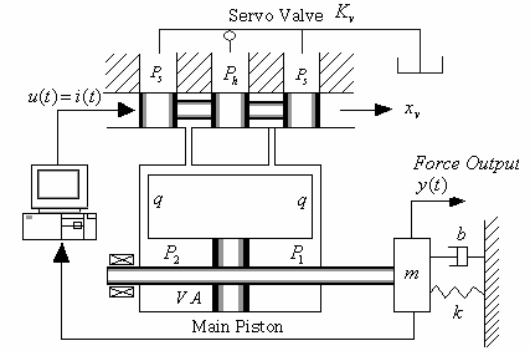

Fig. 6. Hydraulic servo system.

Using Eq. (6), the matrix representation for the total control system can be drawn as shown in Fig. 5.

As shown in Fig. 5, the system has three MISO control structures, and it shows the equivalent 3x3 MIMO feedback control effect. The next procedure is to design controller *G(s)* and pre-filter *F(s)* with the uncertain plant *P(s)*.

4. Mathematical modelling for hydraulic simulator

The hydraulic servo system utilizes electrical current as an input to open the servo valve, and the fluid pressure, which builds according to the opening of the valve, finally moves the actuator to the outside load.

The modeling has three parts: servo valve, hydraulic actuator satisfying continuum equation of oil flow, and load relation from the mechanical cylinder (See Fig. 6).

The transfer function between input current i and output spool velocity x_v can be approximated as a second order system [18]

$$\frac{X_v(s)}{I(s)} = K_v \frac{\omega_n^2}{s^2 + 2\xi\omega_n s + \omega_n^2} \tag{7}$$

where X_v is the spool valve displacement, K_v is a valve gain, ω_n is the natural frequency of the flapper, ξ is the damping ratio, and I represents the input current.

The load pressure P_L represents the pressure difference between each cylinder face, and its mathematical expression is as follows:

$$P_L = P_1 - P_2, P_h = P_1 + P_2, \; P_2 = \frac{P_h - P_L}{2}. \tag{8}$$

If one considers the load pressure, the continuity equation for the q can be the function of spool displacement x_v and load pressure P_L as follows:

$$q = f(x_v, P_L). \tag{9}$$

If we linearize the q around the operating point, it can be represented as

$$q = \left(\frac{\partial q}{\partial x}\right)_0 x_v + \left(\frac{\partial q}{\partial P_L}\right)_0 P_L = C_x x_v - C_p P_L \tag{10}$$

where $C_x = 2c\bar{a}\sqrt{gP_h/\gamma}$, $C_P = c\bar{a}x_{v0}\sqrt{g/\gamma}\Big/\sqrt{P_h}$.

By refining the mathematical model, one can consider the leakage coefficient and compressibility of the fluid as

$$\begin{aligned} q &= q_o + q_c + q_L = A\rho\dot{y} + \frac{\rho V}{K_B}\dot{P}_L + LP_L \\ C_x x &= A\rho\dot{y} + \frac{\rho V}{K_B}\dot{P}_L + (L + C_p)P_L \end{aligned} \tag{11}$$

where q_0 is the incompressible component of the fluid, q_c is the compressible component, q_l is the leakage component, A is the piston area, ρ is the density, K_B is the bulk modulus of the oil, V is the volume of the fluid under compression, and L is the leakage coefficient of the whole system.

The output load F can be represented as

$$F = n_F A P_L \tag{12}$$

where F is the output force and n_F represents the force conversion efficiency. The mechanical parts can be represented as

$$F = M\ddot{y} + B\dot{y} + Ky = n_F A P_L \tag{13}$$

where M is load mass, B is the damping coefficient, and K is the stiffness coefficient.

The transfer equation between input current I and force F for each axis can be obtained as

$$\begin{aligned} P_F(s) = \frac{F(s)}{I(s)} &= \frac{C_x K_v (M s^2 + B s + K)}{a s^3 + b s^2 + c s + d} \\ &= \frac{f s^2 + g s + h}{a s^3 + b s^2 + c s + d} \end{aligned} \tag{14}$$

where $f = C_x K_v M$, $g = C_x K_v B$, $h = C_x K_v K$.

The parameters of *a, b, c, d, f, g* and *h* of Eq. (14) represent the uncertain cylinder characteristics including fluid compressibility, leakage, electrical servo mechanism, non-linear orifice and non-linear mechanical connections. As these parameters are not expressed as fixed constants, parameter varying bounds should be decided. By inspecting the specifications and referencing parameters from other papers, these parameter boundaries are calculated. For a more detailed expression, please refer to Kim et al. [19].

5. Controller design

The QFT is the robust control method used to guarantee stable control action even if the plant has model uncertainty with external input and output disturbances. The required feedback control action can be quantitatively decided by the

Table 1. Varying range of parameter set of plant.

Parameters	Range	Parameters	Range
a_{11}	8.852e-8	b_{11}	3.671e-5~6.264e-5
c_{11}	1.564e-3~1.585e-3	d_{11}	3.664e-3 ~ 6.256e-3
a_{22}	6.019e-8	b_{22}	2.231e-5~3.806e-5
c_{22}	2.538e-3~2.551e-3	d_{22}	2.226~3.801
a_{33}	1.393e-8~5.573e-8	b_{33}	1.999e-4~8.073e-4
c_{33}	8.781e-3~9.391e-3	d_{33}	1.99e-2~2.018e-2
f_{11}	5.937e-2~8.203e-2	g_{11}	4.75e-2~6.563e-2
h_{11}	5.937~8.203	f_{22}	5.937e-2~8.203e-2
g_{22}	5.225e-2 ~7.219e-2	h_{22}	5.937 ~ 8.203
f_{33}	0	g_{33}	0
h_{33}	0.1681		

Table 2. Parameter value of dynamic plant equation.

Parameter	Value	Unit	Description
A_{Lat}	1.526e-3	m^2	Piston area of Lateral axis
A_{Lon}	2.512e-3	m^2	Piston area of Longitudinal axis
A_{Ver}	4.8081e-3	m^2	Piston area of Vertical axis
V_{Lat}	3.8151e-4	m^3	Cylinder Volume of Lateral Axis
V_{Lon}	4.2704e-4	m^3	Cylinder Volume of Longitudinal Axis
V_{Ver}	8.0776e-4	m^3	Cylinder Volume of Vertical Axis
M	100 ~ 500	Kg	Load mass
B	200 ~ 540	Ns/m	Load Damping
K	10,000 ~ 50,000	N/m	Load spring stiffness
L	1.56e-11	m^3/sPa	Leakage coefficient
C	0.6 ~ 0.8		Flux coefficient
g	9.8	m/s^2	Gravity acceleration
P_h	21e6	Pa	Supply pressure
x_v	0.00001 ~ 0.0033	M	Displacement of Spool valve
w	0.008	M	Port width
K_B	1.379e9	Pa	Bulk modulus
ρ	870	Kg/m^3	Hydraulic density
Kv_L	8.25e-5	m/mA	Gain of spool valve (Lateral, Longi)
Kv	0.0825	m/A	Gain of spool valve (Vertical)
n_F	0.9		Force conversion efficiency

design specification represented by (i) stability margin, (ii) tracking specification, and (iii) disturbance rejection specification. These three specifications have the certain boundaries in the complex plane (including amplitude and phase). The uncertain plant, which can be modeled as a template surrounded by the uncertain plant parameters, should be designed by satisfying the above three boundaries in the Nichols chart. Also, the prefilter *F(s)* should be designed to filter out unnecessary disturbances. The typical design process is as follows :

5.1 Design specification

Typical design parameters, such as rising time, overshoot and settling time, should be transferred from the time domain to the frequency domain. The specifications also include the stability margin and disturbance rejection specification.

5.2 Plant template

The three axes road simulator as shown in Fig. 1 has one dummy mass (which can be represented as the suspension unsprung mass of the quarter car model), which is activated by three perpendicular hydraulic cylinders. As explained from the previous section, the servo valve input current *I(s)* and output of cylinder displacement and force *Y(s)* and *F(s)* can be represented, respectively, as

$$P_Y(s) = \left\{ P_{ij}(s) = \frac{e_{ij}}{a_{ij}s^3 + b_{ij}s^2 + c_{ij}s + d_{ij}} \right\} \quad (ij=3) \qquad (15)$$

$$P_F(s) = \left\{ P_{Fij}(s) = \frac{f_{ij}s^2 + g_{ij}s + h_{ij}}{a_{ij}s^3 + b_{ij}s^2 + c_{ij}s + d_{ij}} \right\} \quad (ij=1,2) \qquad (16)$$

where

$$a_{ij} = \frac{VM}{K_B n_F A} \quad , \quad b_{ij} = \left[\frac{VB}{K_B n_F A} + (L + C_P)\frac{M}{n_F A} \right]$$

$$c_{ij} = \left[A + \frac{VK}{K_B n_F A} + \frac{B}{n_F A}(L + C_P) \right], \; d_{ij} = \left[\frac{K}{n_F A}(L + C_P) \right]$$

$$e_{ij} = C_x K_v, \; f_{ij} = C_x K_v M \; , \; g_{ij} = C_x K_v B \; , \; h_{ij} = C_x K_v K$$

and subscript *ij* represents the three axis indices. It is necessary to represent the plant uncertainty in the Nichols chart. The plant template represents the plant uncertainty with parameter variation. The load simulator is the set of the all possible plants with the variation of all parameters of *a, b, c, d, f, g* and *h* in accordance with the changing of load condition as well as spool displacement. The variation boundaries of the uncertain parameters are very important and should be well established to synthesize the good controller. The plant parameter variation of *a, b, c, d, f, g* and *h* are summarized as below:

The hydraulic system parameters are represented byTable 2.

As it is reasonable to set the maximum operating frequency to 300 Hz in considering the slow mechanical plant, the discrete frequency set can be defined as

= [0.1,1,3,5,10,20,30,50,100,200,300].

The uncertain plant sets are drawn on the Nichols chart as shown in Fig. 7.

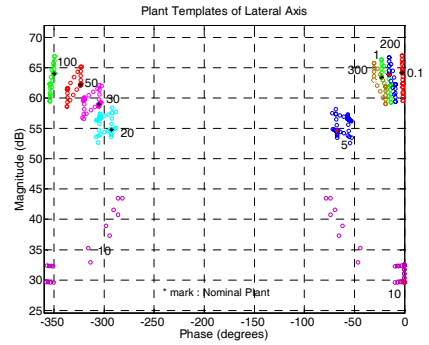

(a) Lateral axis

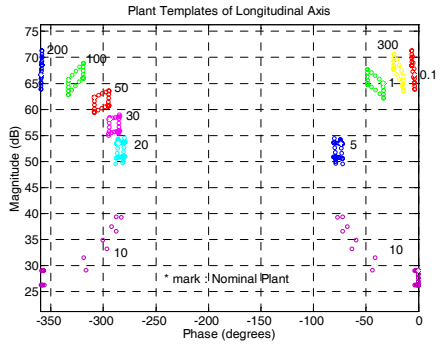

(b) Longitudinal axis

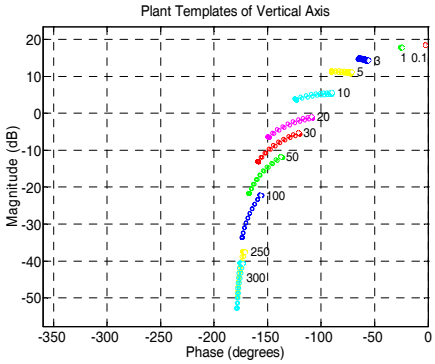

(c) Vertical axis

Fig. 7. Plant templates.

5.3 Boundary condition

Usually, the boundaries are represented by (1) the robust stability

$$\left|\frac{PG}{1+PG}(j\omega)\right| \le 1.2,\ \omega \ge 0 \tag{17}$$

where P is the plant and G is the feedback controller, and (2) the tracking boundary represented by

$$T_U(\omega) \le \left|F\frac{PG}{1+PG}(j\omega)\right| \le T_L(\omega), \tag{18}$$

where T_U is the upper bound and T_L represents the lower bound of the tracking specification. However, as each cylinder has different specifications, the lateral axis upper boundary conditions are M_p = 1.1 (Overshoot 10%), t_s = 0.043s, t_r= 0.012s, lower ones are set as t_s= 0.0778s , t_r= 0.0448s. The obtained upper and lower boundary conditions are represented in the frequency domain as

$$T_{L_U}(j\omega) = \frac{62.5(j\omega+250)}{(j\omega)^2+147.5(j\omega)+15625} \tag{19}$$

$$T_{L_L}(j\omega) = \frac{8.789e7}{(j\omega)^3+15775(j\omega)^2+2.349e6(j\omega)+8.789e7}. \tag{20}$$

The longitudinal axis upper boundary conditions are M_p = 1.1 (overshoot 10%), t_s = 0.082s, t_r= 0.0256s, lower ones are set as t_s= 0.149s , t_r= 0.0836s. The obtained upper and lower boundary conditions are represented in the frequency domain as

$$T_{Lo_U}(j\omega) = \frac{12.25(j\omega+400)}{(j\omega)^2+2\times0.59\times70j\omega+4900} \tag{21}$$

$$T_{Lo_L}(j\omega) = \frac{1.41750e5}{(j\omega+45)(j\omega+45)(j\omega+70)}. \tag{22}$$

Finally, the vertical axis boundary conditions are set as

$$T_{V_U}(j\omega) = \frac{1.323(j\omega+400)}{(j\omega)^2+2\times0.4559\times23j\omega+529} \tag{23}$$

$$T_{V_L}(j\omega) = \frac{3312}{(j\omega+12)(j\omega+12)(j\omega+23)}. \tag{24}$$

5.4 Loop shaping

In order to create an optimal design, the loop should be close to a U-contour for guaranteeing the stability margin. It should be within the given frequency range $L(j\omega)$ and located above the final combined bondaries (i.e. tracking and disturbance rejection boundaries.) Loop shaping is the process with heuristical design. Once the appropriate loop shaping is decided, then the final controller and filter are synthesized. An initial integrator is used then appropriate gain adjustment, zero and pole are added. In this paper, the lateral and longitudinal axes have included notch filters for better loop shaping. The final loop shapings are shown in Fig. 8.

5.5 Controller design

After loop shaping, the final controllers for each axis can be calculated as

$$\begin{aligned} G_L(s) &= K\frac{1}{s^n}\frac{s/z+1}{s/p+1}\frac{s^2/\omega_n^2+2\zeta_1 s/\omega_n+1}{s^2/\omega_n^2+2\zeta_2 s/\omega_n+1} \\ &= \frac{(s/10+1)(s^2/10^2+2\times0.5s/10+1)}{s(s/4+1)(s^2/10^2+2\times0.04s/10+1)} \end{aligned} \tag{25}$$

$$G_{Lo}(s) = \frac{0.87(s/100+1)(s^2/10^2+2\times0.5s/10+1)}{s(s/15+1)(s^2/10^2+2\times0.04s/10+1)} \tag{26}$$

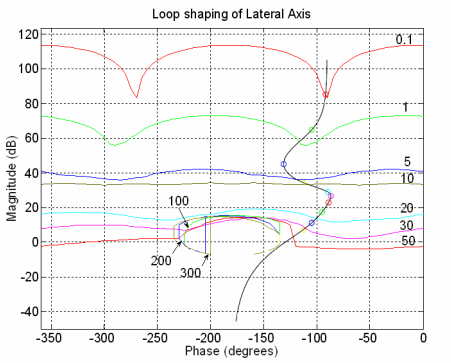

(a) Lateral axis

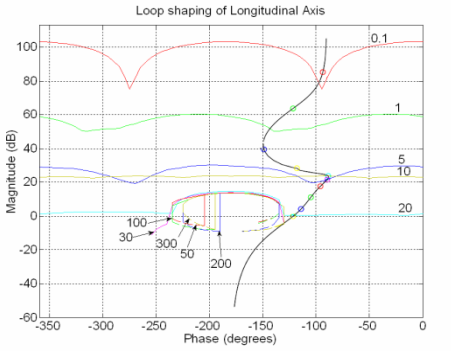

(b) Longitudinal axis

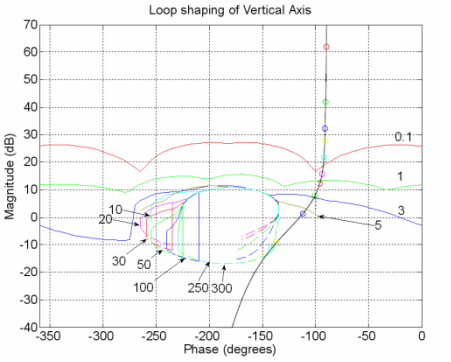

(c) Vertical axis

Fig. 8. Controller design of three-axes axis.

$$G_V(s) = K\frac{1}{s^n}\frac{s/z+1}{s/p+1}\frac{s/z+1}{1} = \frac{15(s/2.48+1)(s/40+1)}{s(s/240+1)}. \quad (27)$$

where $G_L(s)$ and $G_{Lo}(s)$ are the lateral and longitudinal axis controllers, repectively, and $G_V(s)$ represents that of the vertical axis. The final controllers obtained from QFT show maximum 4th order transfer functions, which are comparatively low order functions because other robust control methods, such as H_2/H_∞ or μ synthesis, have much higher controller orders, rendering the real-time control difficult to implement.

5.6 Pre-filter design

Finally, the pre-filter is introduced in consideration of the working range of the cylinders. The pre-filter is designed in accordance with real road simulator specification. The designed pre-filters are shown in Fig. 9 in the frequency domain and their equations are represented by

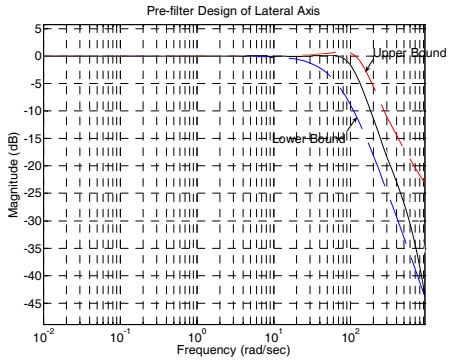

(a) Lateral axis

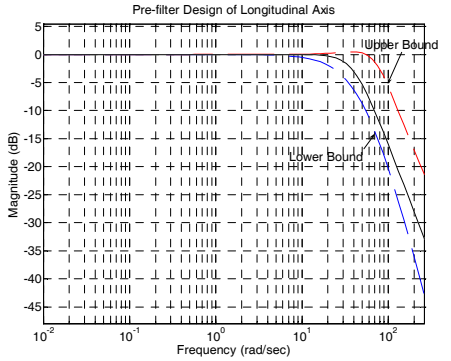

(b) Longitudinal axis

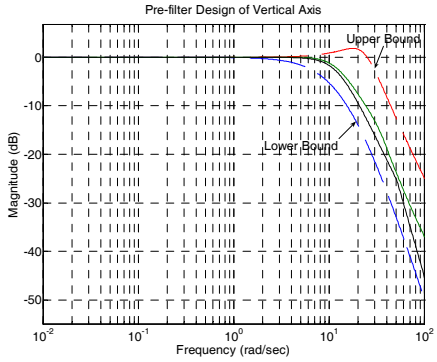

(c) Vertical axis

Fig. 9. Pre-filter design of vertical axis.

$$F_L(s) = \frac{1}{s^2/\omega_n^2 + 2\zeta s/\omega_n + 1} = \frac{1}{s^2/100^2 + 2\times 0.6\, s/100 + 1} \quad (28)$$

$$F_{Lo}(s) = \frac{1}{s^2/40^2 + 2\times 0.707\, s/40 + 1} \quad (29)$$

$$F_V(s) = \frac{1}{s^2/11^2 + 2\times 0.6\, s/11 + 1}. \quad (30)$$

The figures show that the controller will satisfy the uncertain plant dynamics within the upper and lower bounds.

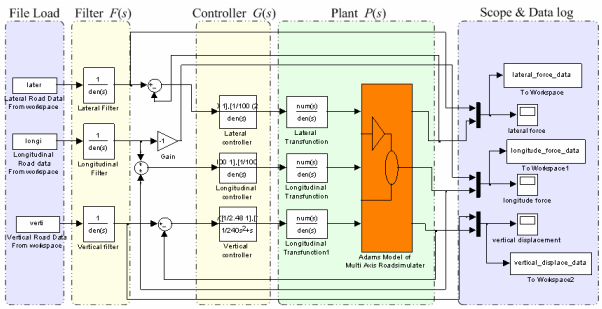

Fig. 10. Co-simulation model of multi-axes hydraulic simulator.

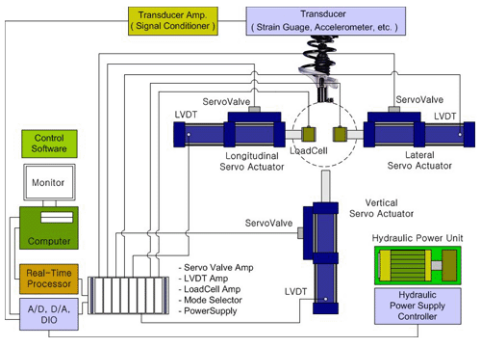

Fig. 11. Schematic diagram for the experiment.

6. Simulation results

The Adams model is shown in Fig. 1 and its corresponding simulation and experimental diagram are shown in Fig. 10 and Fig. 11. The simulator uses the force control for the longitudinal and lateral axes and displacement control is utilized for the vertical axis. The simulation is performed simultaneously using the Adams model and Matlab/Simulink software. Real road data is used as the input signal.

Fig. 12 shows the results of each axis simulation. Fig. 12(a) and 12(b) show the force response for the longitudinal and lateral axes, respectively, and Fig. 12(c) represents the displacement for the vertical axis response. Each axis shows the maximum RMS errors of 0.20%, 0.85% and 0.13%, respectively, and these results prove that the proposed controller works very well to reproduce the random road data. Although there is minor coupling between the vertical lateral and longitudinal axes (about 3% as explained in Section 2), this coupling is safely negligible. Therefore, the independent controller can reproduce the input motion accurately. The results also show that the proposed controller is robust even though there are negligible external disturbances which are considered as coupling effects between each axes.

7. Experimental results

The road simulator input signal shows road fluctuation, and its major frequency range is usually between 2 Hz – 40 Hz. It also has random characteristics. In the real experiment, we

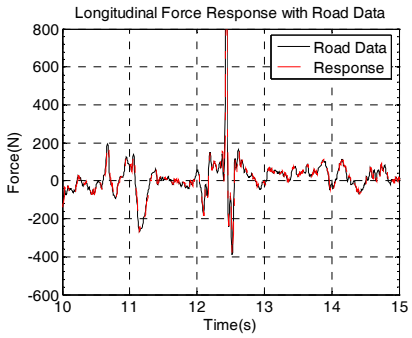

(a) Longitudinal force response with real road data excitation

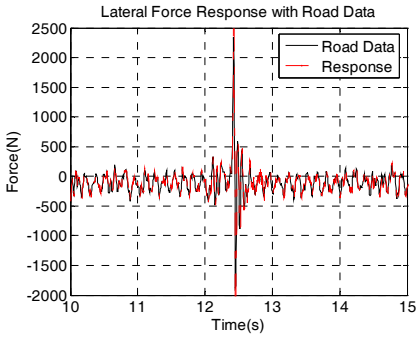

(b) Lateral force response with real road data excitation

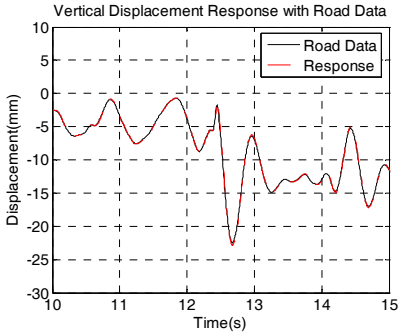

(c) Vertical displacement response with real road data excitation

Fig. 12. Co-simulation results of the three axes with real road data.

chose an exciting random input signal with a maximum of 40 Hz to actuate the simulator. The experimental test rig is shown in Fig. 13.

The test specimen is the front suspension a Korean automotive maker's compact car (the lower control arm with nonlinear bushings and ball joint). Displacement and force controls are made through the ball joint of the LCA. The load cells are attached as a force sensor, and LVDT is used as a displacement one. 200 bars of pressure are applied to the cylinder.

We made a GUI using Labview software for real-time control and its result is shown in Fig. 14. In the figure, the white line represents the random input signal and the red represents the controlled cylinder response output. The experimental result shows that the proposed controller tracks well up to 40 Hz.

After testing under various input conditions and saving the

Fig. 13. The real plant of dynamic road simulator.

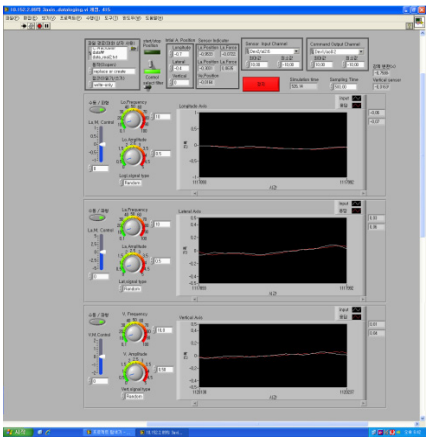

Fig. 14. Designed software using Labview andIts result.

input and output signals, we reproduced one of the results as shown in Fig. 15. In Fig. 15 the black solid line is the input signal, and blue dashed line represents the cylinder output response. Fig. 15 (a) is the longitudinal force response and its maximum RMS error is 4.55%. Fig. 15 (b) is the lateral force reponse output and its maximum RMS error is 5.38%. Fig. 15 (c) shows the vertical displacement response and its corresponding maximum RMS error is 7.64%. Although the maximum RMS error shows a slightly larger value compared to the simulated results, it is satisfactory because the commercialized road simulator permits a reproduced maximum RMS error of 9% (Jeong, [17]). The RMS error difference between the simulated response and experimental one is considered mainly due to the plant modeling error and hydraulic pump's supply fluid flow rate shortage. The pump's supply fluid flow rate is very important to engage the real road with enough cylinder force, but in our experiment, the supply flow rate is a slightly insufficient because the small fluid pump used in the experimenthas a capacity that is usually suitable for one axis actuation.

The relative tracking errors of each axis in Fig. 15 is shown in Fig. 16. In Fig.16, the black solid line, the blue dashed line and the brown dash-dotted line represent the relative tracking error of the longitudinal axis, the lateral axis and vertical axis, respectively. The relative tracking errors of the experimental

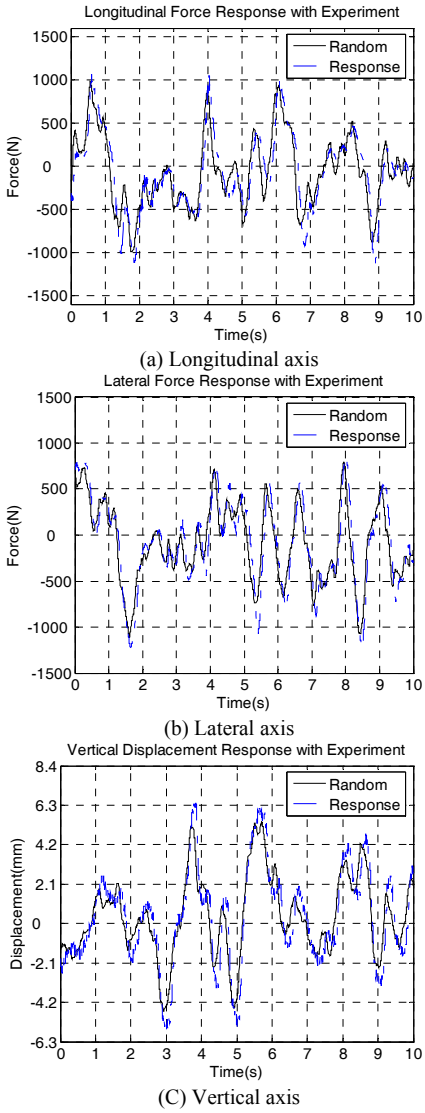

Fig. 15. Random responses of experiment with multi-axes hydraulic simulator.

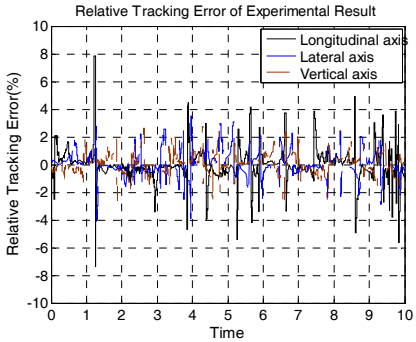

Fig. 16. Relative Tracking Errors of 3-axes on Fig.15.

results of the threeaxes are within 3%.

8. Conclusion

We designed the robust controller for the three-axis road

simulator, which has the uncertain parameters of fluid compressibility, fluid leakage, electrical servo components, and non-linear mechanical connections. In designing the 3x3 MIMO system controller, three equivalent MISO systems are used and its verifications are made from dynamic simulation result as well as mathematical derivation. By applying the QFT algorithm to each MISO system, which satisfies the amplitude and phase design boundaries such as stability, tracking, and disturbance rejection, the three robust controllers are synthesized with pre-filters. The obtained controllers have low order transfer functions (maximum 4^{th} order), which is another benefit to implement testing in the real-time environment.

The simulation and experimental results show that the proposed method can work well in controlling the hydraulic simulator with maximum RMS errors of 0.67% and 7.64%, respectively. Therefore, the proposed method of three MISO controllers can be considered to satisfy the stability margin, tracking performance as well as rejecting the external disturbance for the uncertain hydraulic plant. This method can potentially be applied to the hydraulic road simulator and yield satisfactory results.

Acknowledgement

The authors are thankful to JKS Co. in Gwangju, Korea, for their technical support and operational help for the three-axis simulator.

References

[1] J.A. Jung and J.C. Lee, A Study of Lab Simulation using Road simulator at the road riding of the vehicle, *Asia Motors Technical Review* (1990) 73-85.

[2] I.M. Horowitz, *Synthesis of Feedback Systems*, Academic Press, New York (1963).

[3] I.M. Horowitz and M. Sidi, Synthesis of feedback systems with large plant ignorance for prescribed time-domain tolerance, *Int. J. Control*, 16 (2) (1972) 287-309.

[4] I.M. Horowitz, Improved Design Technique for Uncertain Multi Input Multi Output Feedback Systems, *Int. J. Control*, 36 (6) (1982) 977-988.

[5] J.J. D'Azzo and C.H. Houpis, *Linear Control System Analysis*, McGraw - Hill Inc. (1988).

[6] I.M. Horowitz, *Quantitative Feedback Theory (QFT)*, QFT Publication, 4470 Grinnell Ave, Boulder, Colorado, 80303 (1992).

[7] O. Yaniv and I.M. Horowitz, A Quantitative Design Method for MIMO Linear Feedback Systems Having Uncertain Plants, *Int. J. Control*, 43 (1986) 402-421.

[8] Y. Chait and C.V. Hollot, A Comparison Between H_∞ Methods and QFT for a single-loop Plant with Both Parametric Uncertainty and Performance Specifications, *Recent Development in Quantitative Feedback Theory*, *ASME WAM Config*., O.D.I. Nwokah, ed. (1990) 33-40.

[9] R. Zang, Alleyene and E. Prasetiwan, Modeling and H_2/H_∞ MIMO Control of an Earthmoving Power Train, *ASME, J. of Dynamic Systems, Measurement and Control*, 124 (4) (2002) 625-636.

[10] J. G. Ziegler and N. B. Nichols, Optimum Settings for Automatic Controllers. *ASME Trans.,* 64 (1942) 759-768.

[11] U. Shaked, I. M. Horowitz and S. Glode, Synthesis of Multivariable Basically Non-interacting Systems with Significant Plant Uncertainty, *Automatica*, 12 (1976) 61-71.

[12] C. Borghesani, *Computer Aided Design of Robust Control Systems Using the Quantitative Feedback Theory*, M.S. Thesis, Mechanical Engineering Department, University of Massachusetts, Amherst, MA. (1993).

[13] Y. Chait and O. Yaniv, *Quantitative Feedback Theory Toolbox User's Guide*, Terasoft Inc., (1993-2003).

[14] M. S. Park and J. W. Lee, Direct Multivariable Quantitative Feedback Theory, *KSME*, 22 (3) (1998) 562-568.

[15] K. K. Ahn, N. H. T. Chau and D. Q. Truong, Robust force control of a hybrid actuator using quantitative feedback theory*, JMST*, (2007) 2048-2058.

[16] Q. P. Ha, Q. H. Nguyen, H. F. Rye and H. F. Durrant-Whyte, Impedance control of a hydraulically actuated robotic excavator, *Automation IC*, (2000) 421-435.

[17] S. Jeong, J. Kim and S. Ryu, A Study on Operational Software Development and Calibraiton of Multi-axis Vibrating Testing Device, *Transactions of KSAE*, 9 (2) (2001) 143-151.

[18] W. J. Thayer, *Transfer Functions for Moog Servo valves*, Moog Inc. (1965).

[19] J. W. Kim, D. J. Xuan and Y. B. Kim, Design of Forced Control System For a Dynamic Road Simulator, , *International Journal of Automotive Technology*, (2008) 37-43.

Jin-Wan Kim received his B.S. degree in Aerospace Engineering from Chosun University, South Korea in 1990. He then received his M.S. degree in Aerospace and Mechanical Engineering from Korea Aerospace University, South Korea in 2003 and his Ph.D degree in Mechanical Engineering from Chonnam National University, South Korea in 2008. He is currently a president of Advanced Mechatronics Technology in Gwangju, Republic of Korea.

Dong-Ji Xuan received his B.S. degree in Mechanical Engineering from Harbin Engineering University, China in 2000. He then received his M.S. and Ph.D. degrees in Mechanical Engineering from Chonnam National University, South Korea in 2006 and 2009, respectively. Currently, he is a faculty of the Department of Mechanical Engineering, Wenzhou University, China. His research interests include control and optimization of PEM fuel cell system, dynamics and control, and mechatronics.

Young-Bae Kim received his B.S. degree in Mechanical Design from Seoul National University, South Korea in 1980. He then received his M.S. degree in Mechanical Engineering from the Korean Advanced Institute of Science and Technology (KAIST), South Korea in 1982 and his Ph.D. degree in Mechanical Engineering from Texas A&M University, USA in 1990. Dr. Kim is currently a Professor of the School of Mechanical and Systems Engineering in Chonnam National University, South Korea. Dr. Kim's research interests include mechatronics, dynamics and control, and fuel cell hybrid electric vehicle (FCHEV) systems.